

# A spectroscopic study of the $\delta$ Scuti star $\rho$ Puppis<sup>\*</sup>

P. Mathias<sup>1</sup>, D. Gillet<sup>2</sup>, C. Aerts<sup>3, \*\*</sup>, and M.G. Breitfellner<sup>4</sup>

<sup>1</sup>Observatoire de la Côte d'Azur, Département Fresnel, U.M.R. 6528, BP 4229, F-06304 Nice Cedex 04, France

<sup>2</sup>Observatoire de Haute-Provence, CNRS, F-04870 Saint-Michel l'Observatoire, France

<sup>3</sup>Instituut voor Sterrenkunde, Katholieke Universiteit Leuven, Celestijnenlaan 200B, B-3001 Heverlee, Belgium

<sup>4</sup>ISO Science Operations, ESA/VILSPA Satellite Tracking Station, PO Box 50727, E-28080 Madrid, Spain

Received 18 March 1997 / Accepted 21 July 1997

**Abstract.** We present a spectroscopic analysis of the  $\delta$  Scuti star  $\rho$  Pup on the basis of high resolution data spread over 4 consecutive nights. Despite the clearly sinusoidal shape of the radial-velocity curves, cycle-to-cycle variations are observed. A frequency analysis points towards the already known frequency  $\nu_0 = 7.098168 \text{ c.d}^{-1}$  assigned to a radial mode and towards two possible secondary non-radial oscillations at  $\nu_1 = 7.8 \text{ c.d}^{-1}$  and  $\nu_2 = 6.3 \text{ c.d}^{-1}$  of much smaller amplitude.

Using the moment method we confirm that the main oscillation is a radial mode. The second mode is found to be axisymmetric, but because of its small amplitude and our relatively small data set, no more detailed information on its pulsation parameters could be derived. The third frequency, if real, corresponds to a non-axisymmetric mode.

The running wave effect may be present between the Fe I and  $H\alpha$  lines, the latter being late by about 0.5 % of the pulsation period. No evidence is found in our observed profiles (Ca I, Fe I,  $H\alpha$ ) for a shock wave mechanism as previously suggested by Dravins et al. (1977). New observations are required to confirm the presence of a period-dependent shock wave which should be of weak intensity.

**Key words:** stars: oscillations – stars: variables:  $\delta$  Scuti – stars: individual:  $\rho$  Pup

---

## 1. Introduction

The light variability of  $\rho$  Pup (HD 67523, F6 II) was first announced by Eggen (1956), who measured a total amplitude of 0.15 mag. The author classified this star as a  $\delta$  Scuti type variable. It has one of the lowest effective temperatures of all known stars of this class. This star represents a particular branch of the

$\delta$  Scuti variables, having a relatively large radial-velocity amplitude (Kurtz et al. 1995). In 1956, Struve et al. showed that the radial velocity variation had a peak-to-peak amplitude of  $10 \text{ km.s}^{-1}$  and that the maximum brightness occurred approximately 0.02 days later than the minimum radial velocity. The authors also pointed out that the amplitude and the shape of the heliocentric radial-velocity curve was probably constant.

Ponsen (1963) analysed a large photometric data set and found a period  $P = 0.1408806 \text{ d}$ . The author also analysed radial-velocity data and found a period  $P = 0.1408814 \text{ d}$  (corresponding to a frequency  $\nu_0 = 7.098168 \text{ c.d}^{-1}$ ), falling within the mean error of the photometric period value. Despite the fact that some of the observed light-curves deviated systematically from the mean curve at certain phases (the largest difference is 0.01 mag), no superposed periodicity was found by the author. From low-resolution spectral measurements, Trodhal & Sullivan (1977) derived night-to-night differences in the amplitude of the temperature variations, but due to their perfectly periodic light curve, they could not appeal to a varying pulsation amplitude. One of their conclusions was that the star might pulsate apherically.

Dravins et al. (1977, hereafter DLS) suggested that  $\rho$  Pup, like most other  $\delta$  Scuti variables, had other small-amplitude variations besides the one with the main period. They observed a secondary bump on the radial-velocity curve, occurring near maximum inward velocity. Together with the presence of *transient* Ca II K emission just before the maximum acceleration, the authors invoked a shock-wave mechanism as the one usually modeled in the case of RR Lyrae stars. This scenario is compatible with the radial character of the pulsation mode of the star (e.g. Campos & Smith 1980). Fracassini et al. (1983) observed permanent UV Mg II *h* and *k* emissions with a larger strength near maximum light. They found that the chromosphere and the photosphere oscillate in phase, while there is a possible phase opposition if an extended atmosphere is considered. A stratification effect is also noticed by Buscombe (1957) who measured some departures of the radial-velocity curves for lines produced at different chromospheric levels in the photosphere near the maximum light. Finally, Yang et al. (1987) observed

---

\* Based on observations obtained at the European Southern Observatory, Chile

\*\* Postdoctoral Fellow, Fund for Scientific Research, Flanders, Belgium

that all the radial-velocity curves are in phase, except the one corresponding to He I  $\lambda\lambda$  8750, which is late by about 4 minutes.

The aim of this paper is to give an up-to-date observational status of  $\rho$  Pup using high-quality spectroscopic observations. Our data are described in Sect. 2 and a rough analysis is given in Sect. 3. The pulsation parameters are derived in Sect. 4, and stratification effects associated to a running wave phenomenon are searched for in Sect. 5. In Sect. 6, we discuss the shock wave scenario of DLS. Finally, some concluding remarks are given in Sect. 7.

## 2. Observations and data reduction

The spectroscopic observations used in this study were obtained with the Coudé Echelle Spectrograph (CES) at the 1.4 m CAT telescope at ESO (La Silla, Chile). The detector used was a CCD LORAL 2048, with  $2048 \times 2048$  elements of size  $15 \times 15 \mu\text{m}^2$ . The observations were performed during four nights in February 1995 (21, 22, 23 and 24) and covered three spectral regions: around  $H\alpha$  (first and last night), around some iron lines ( $\lambda\lambda$  6393, second night) and around Ca I ( $\lambda\lambda$  6122, third night). The resolving power  $\lambda/\Delta\lambda$  was around 60 000 for all the considered spectral domains, leading to a velocity resolution of about  $5 \text{ km.s}^{-1}$ . During the two first nights, the weather was not very good, and the exposure time was around 3 minutes. The conditions during the last two nights were better, allowing a decrease of the exposure time down to 1.5 minutes. This ensured a signal-to-noise ratio around 200. The star was observed during 4.4 h the first night, while it was observed during 7 h the three other nights.

Each spectrum was corrected for the pixel-to-pixel response through division by the mean of 5 flat field spectra that were obtained using an internal lamp. This ensures a good correction since the related optical path is the same as the stellar one. The wavelength calibration was done using about 20 lines of a thorium lamp. Then, the spectra were normalized to the continuum by a cubic spline function. Finally, in order to get them in the heliocentric frame, they were corrected for the Earth motion using the BARVEL subroutine (Stumpff 1980).

## 3. Data analysis

### 3.1. Radial-velocity curves

The radial-velocity curves have been obtained using a gaussian fit of the whole profile except in the case of  $H\alpha$ , which has a broad profile with well-marked Stark wings. In the latter case only the core of the line was considered. In all cases, the resulting velocity curves show clearly a sinusoidal shape, as illustrated in Fig. 1 for the  $H\alpha$  line. A least-squares sine-fit of the different elements of all nights, with the imposed frequency  $\nu_0 = 7.098168 \text{ c.d}^{-1}$  (Ponsen 1963) provided the barycentric average velocity in the heliocentric frame  $\bar{v}$  and the peak-to-peak amplitude 2K of the variation. The results are:

$$\begin{cases} \bar{v} = 47.11 \pm 0.59 \text{ km.s}^{-1}, \\ 2K = 8.39 \pm 0.76 \text{ km.s}^{-1}. \end{cases} \quad (1)$$

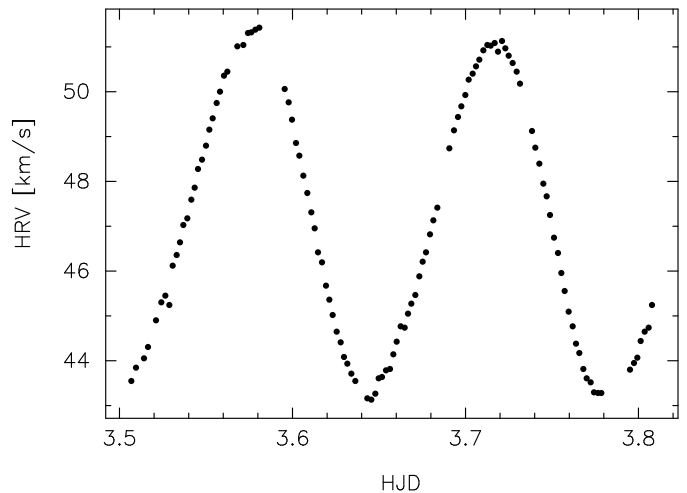


**Fig. 1.** Heliocentric radial-velocity curve as a function of the heliocentric Julian day (from which 2 449 770 has been subtracted) for the  $H\alpha$  line measured on night February 24<sup>th</sup>, 1995

The value of the average velocity is slightly larger than the one already reported by different authors, which is about  $46 \text{ km.s}^{-1}$  (Struve et al. 1956), whereas the 2K-amplitude is somewhat smaller than usually given in the literature (we found values between 9 and 11  $\text{km.s}^{-1}$ , Danziger & Kuhl 1966, Campos & Smith 1980). The values of the two above parameters associated to a given night or a given element are found to be slightly variable, mostly within the error bars. This is partly due to blend phenomena but can also be caused by the projection factor, which takes into account the geometrical projection, the limb-darkening effect, and the velocity gradient within the line forming region (Mathias et al. 1994).

As shown on Fig. 1 (or on Fig. 4d for the Ca I line), the heliocentric radial-velocity curve does not present any definite secondary bump near the minimum, contrary to what is concluded in DLS. DLS suggested that this bump could not be seen in earlier studies due to insufficient time resolution. Our time resolution being the best ever obtained on this star, the reality of this bump is not supported by our observations.

### 3.2. Frequency analysis

Yang et al. (1987) also reported night-to-night variations of the radial velocity, and invoked the presence of a low-amplitude long beat period. The presence of an additional oscillation should not be surprising since multiple periods often appear in  $\delta$  Scuti stars. Despite the fact that our data cover only four consecutive nights, we searched for a second frequency, using the PDM algorithm developed by Stellingwerf (1978) and the CLEAN algorithm of Roberts et al. (1987). We had first to define an homogeneous data set, containing only radial velocities of well-measured, unblended lines. We thus used only the  $H\alpha$ , Fe I  $\lambda\lambda$  6393 and Ca I  $\lambda\lambda$  6122 lines. The resulting set contains about 330 radial-velocity data. The frequency  $\nu_0$  is easily recovered, with a minimum in the  $\Theta$ -statistics of 0.15.

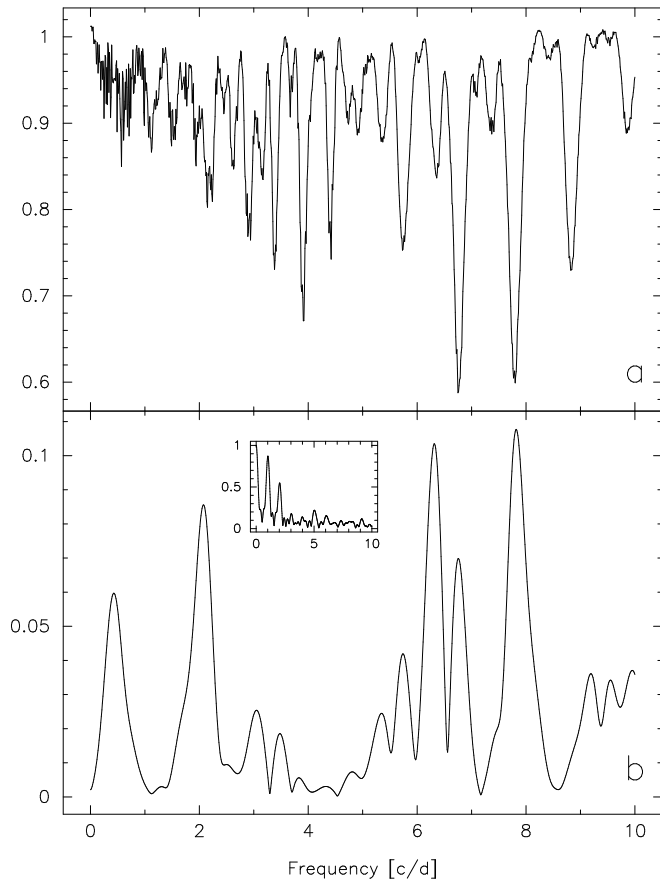


**Fig. 2.** **a** The  $\Theta$ -statistics for the residuals of the radial velocity, after prewhitening with frequency  $\nu_0$  using a (5,2) bin structure. Note the two minima which correspond to a one-day alias of each other. **b** The CLEAN spectrum obtained from the same data set. The used gain is 0.5, and 50 iterations were performed. The small graph inside represents the spectral window

After prewhitening the data with  $\nu_0$ , we have computed the  $\Theta$ -statistics and the CLEAN spectrum for the residuals. The result is shown on Fig. 2. On the PDM analysis, two minima are found, with a  $\Theta$ -value of about 0.6, which are separated by about  $1 \text{ c.d}^{-1}$ . They are aliases of each other. The ambiguity between these two frequencies should be removed by the use of the CLEAN algorithm. Indeed, the aliases correspond, on the CLEAN power spectrum, to two unequal peaks, the largest being centered around  $\nu_1 = 7.815 \pm 0.087 \text{ c.d}^{-1}$ . This frequency accounts for 44% of the variance of the residuals. In order to discriminate between these two aliases, we performed a sine-fit to the data prewhitened with the frequency  $\nu_0$ , using both the  $\nu_1$  and  $\nu_1 - 1$ . It appears that the variance fraction corresponding to  $\nu_1$  is about 51% while it is around 19% for  $\nu_1 - 1$ . However, the prewhitening of the data with the frequency  $\nu_0$  alters the power distribution, depending on the shape of the spectral window. So, it would be more significant to compare the fit of the original data simultaneously with frequencies  $\nu_0$  and  $\nu_1$ , and alternatively with frequencies  $\nu_0$  and  $\nu_1 - 1$ . This method confirms the above results. Indeed, while frequency  $\nu_0$  accounts for

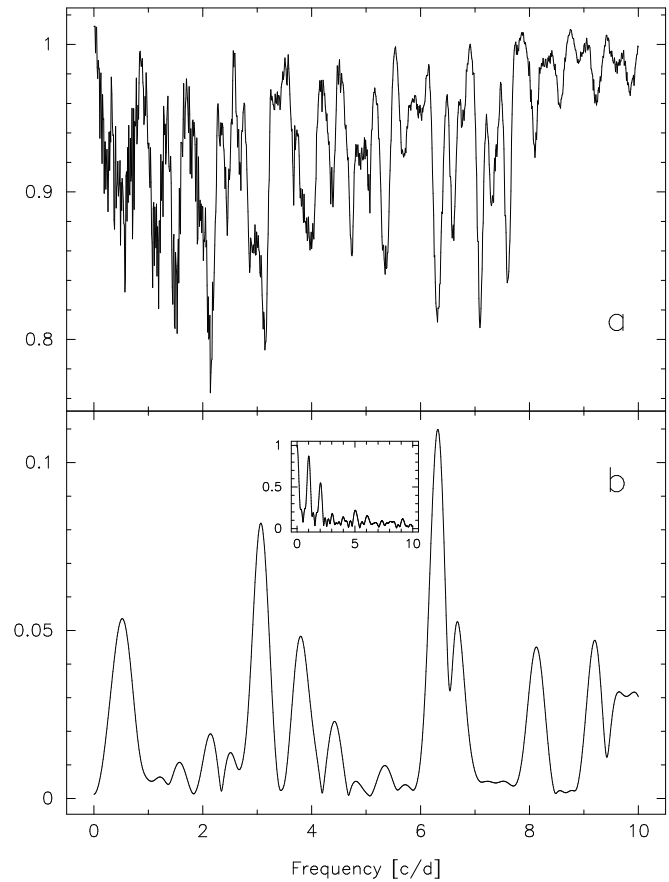


**Fig. 3a and b.** Same as Fig. 2, but after the data set is prewhitened with the frequencies  $\nu_0$  and  $\nu_1$

**Table 1.** For the three detected frequencies are given the 2K-amplitude ( $\pm 0.1 \text{ km.s}^{-1}$ ) together with the fraction of variance of a sine-fit on our data.

	$\nu$ [ $\text{c.d}^{-1}$ ]	2K [ $\text{km.s}^{-1}$ ]	fraction [%]
$\nu_0$	7.098168	8.6	96.6
$\nu_1$	7.815	0.8	2.1
$\nu_2$	6.314	0.4	0.7

97.7% of the variance in both cases, frequency  $\nu_1$  accounts for 2.9% when frequency  $\nu_1 - 1$  accounts for 2.3% of the variance. The latter frequency leading to a worst fit, it will thus not be considered further in this study.

As can be noticed on Fig. 2b, there is an important secondary peak around  $\nu_2 = 6.314 \pm 0.073 \text{ c.d}^{-1}$ , appearing not so well-marked on Fig. 2a, with a  $\Theta$ -value around 0.84. However, this frequency shows a well-defined peak with both methods after prewhitening the data set with  $\nu_0$  and  $\nu_1$ , and it accounts for 18% of the remaining variance (Fig. 3).

The results of the frequency analysis on the complete data set are summarized in Table 1.

The fact that our data set consists of different lines that may be differently affected by the pulsation motion may limit the accuracy of our frequency search. However, such a situation

has already been encountered previously (Mathias et al. 1994) and led to a correct solution in that particular case. Moreover, the detected periods are of the order of 3 h, i.e. well inside the length of a typical observing night (7 h). Finally, the amplitude connected to the frequency  $\nu_1$  is larger than the dispersion associated to the sine-fit computed on different lines using the frequency  $\nu_0$  alone ( $0.2 \text{ km.s}^{-1}$ ). We are therefore confident that the secondary frequency  $\nu_1$  is real. The reality of  $\nu_2$ , however, remains ambiguous.

The beat-periods with respect to the primary one are respectively 1.40 and 1.28 d. Since we have only a time-spread of 4 days, our frequency determination is not very accurate. Nevertheless, we are able to derive that the three frequencies are not equidistantly splitted ones.

This multiperiodic behaviour encouraged us to undertake a re-analysis of Ponsen's (1963) photometric data. Indeed, these latter are very numerous (about 700 measurements) and well-spread for this purpose: a first set was obtained over three consecutive nights, with an average of 100 observations per night, and a second set, 70 days later, over six nights covering nine days, with an average of 70 observations per night. However, no evidence of any secondary period was given by both used frequency algorithms. An analysis of the two individual parts leads to two very different  $\Theta$ -statistics and CLEAN spectra, with no overlapping structure. The amplitude of the secondary variation is probably too small to be detected photometrically. New data are needed to refine the value of the two secondary frequencies.

### 3.3. Behaviour of the Ca I line profile

Despite the fact that the following results could be derived from other lines, only the Ca I line will be used to illustrate this section. Indeed, this line is unblended and strong, and therefore results should be more conclusive. Fig. 4 represents the residual flux (RF), full-width-at-half-maximum (FWHM) and equivalent-width (EW) variations together with the heliocentric radial-velocity curve (HRV). First, it can be noticed that the HRV curve shows a sinusoidal shape, while the three other variations do not. The HRV curve presents two equivalent maxima, whereas the first maximum is slightly lower than the second one for the FWHM curve, and the opposite situation is found for the RF curve. The FWHM and EW curves vary in the same way, the second one being slightly late compared to the first one. The two maxima of the RF variation are separated by about 0.12 d. Whereas the first RF maximum appears before the corresponding FWHM and EW ones by about 0.09 d, the second maximum is late by about 0.04 d. Unfortunately, our data set is too limited to undertake a frequency analysis. But it should be noted that this apparently different periodic behaviour has already been encountered in the case of the prototype star of the  $\beta$  Cephei variables (Aerts et al. 1994). A frequency analysis of the RF, FWHM, and EW variations of  $\beta$  Cephei showed that their main detected frequency corresponds to the third one in the HRV variations. This was at first interpreted as due to the fact that the main frequency of the line parameters other than the HRV is assigned to a non-radial mode, which affects the line

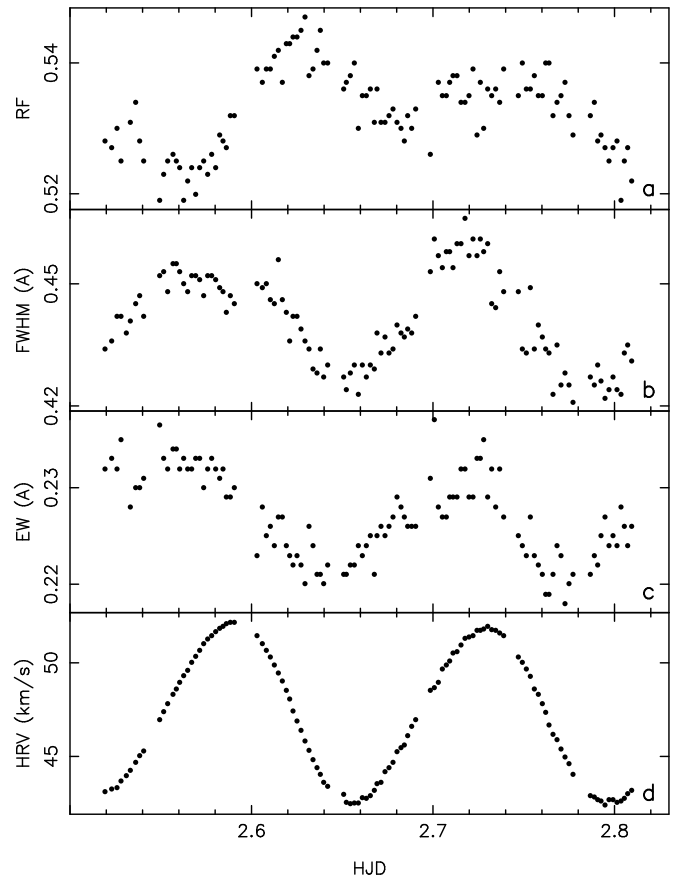


**Fig. 4.** a RF, b FWHM, c EW and d HRV variations for the Ca I  $\lambda\lambda$  6122 profile, as a function of the heliocentric Julian day (from which 2 449 770 has been subtracted)

parameters more than a radial mode (Aerts et al. 1994). More recently, Telting et al. (1997) found that this frequency is the lowest one of a quintuplet due to magnetic splitting of the main mode and corresponds to a spherical harmonic  $(\ell, m) = (2, 2)$ , which indeed results in larger FWHM variations.

Thus, the different variations of the line parameters indicate the presence of at least one non-radial pulsation mode in  $\rho$  Pup.

## 4. Application of the moment method

The ratio of the radial-velocity amplitude to the light one available in the literature ranges from  $76 \text{ km.s}^{-1}.\text{mag}^{-1}$  (Ponsen 1963) to  $93 \text{ km.s}^{-1}.\text{mag}^{-1}$  (Yang et al. 1987). These values, together with a pulsation constant around 0.04 d (Tsvetkov 1984), indicate that  $\rho$  Pup is a radial pulsator in the fundamental mode. Only Danziger & Kuhl (1966) derived a much smaller Q-value, of the order of 0.006 d, by means of the parallax of the star. Their value corresponds to a much higher overtone pulsation. Campos & Smith (1980) used a line-profile-fitting technique to derive that only radial pulsation fits the spectral variations.

In order to derive more precisely the pulsation parameters, not provided in previous studies, we used the moment method, first introduced by Balona (1986) and further developed by Aerts

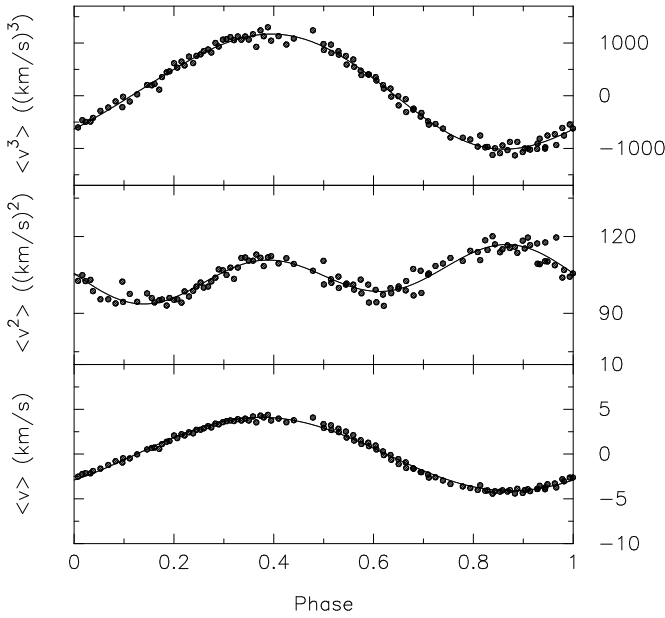


**Fig. 5.** The first three moments of the Ca I line at 6122.21 Å obtained on Feb. 23, 1995. Phases correspond to the frequency  $\nu_0$

(1996, and references therein) on our data set. Among other properties, this method can give an indication of the presence of secondary low-amplitude oscillation modes (Aerts et al. 1994, Mathias & Aerts 1996). In order to apply the moment method, we need to consider unblended lines with clean wings. For the first and the last night, we had not much choice in picking a suitable spectral line due to the broad  $H\alpha$  wings. We considered the moments of the Fe I line at 6546.24 Å, although this line is blended with another Fe I line. The spectra of the second night are of too low quality to accurately determine moments, so we did not consider them in our analysis. For the 23<sup>rd</sup> of February, we picked out the Ca I line at 6122.21 Å.

The first three moments of the lines were calculated and normalised in the usual way (see Aerts et al. 1992). They are shown as dots in the phase diagrams presented in Figs. 5 and 6. The full lines are Fourier fits to the moments according to their time dependence obtained by Aerts (1996), i.e. with zero, one, two harmonics of  $\nu_0$  in respectively  $\langle v \rangle$ ,  $\langle v^2 \rangle$ ,  $\langle v^3 \rangle$ . The quality of the moments is slightly better for the third night than for the first and last night. This is due to the blended nature of the 6546.24 Å line, which also results in a larger FWHM and  $\langle v^2 \rangle$ . For this reason, we used the moments of the third night to study the mode with frequency  $\nu_0$ . For both sets of moments, we observe a double wave nature in the second moment. This points towards the presence of an axisymmetric mode (De Pauw et al. 1993).

We used the discriminant described by Aerts (1996) to identify the mode with frequency  $\nu_0$ . In order to do so, we need to determine the ratio of the horizontal to vertical velocity amplitude. This is done by means of the expression  $GM/\nu_0^2 R^3$  with  $M = 1.7 M_\odot$  (Trodahl & Sullivan 1977) and  $R = 4 R_\odot$  (Dravins

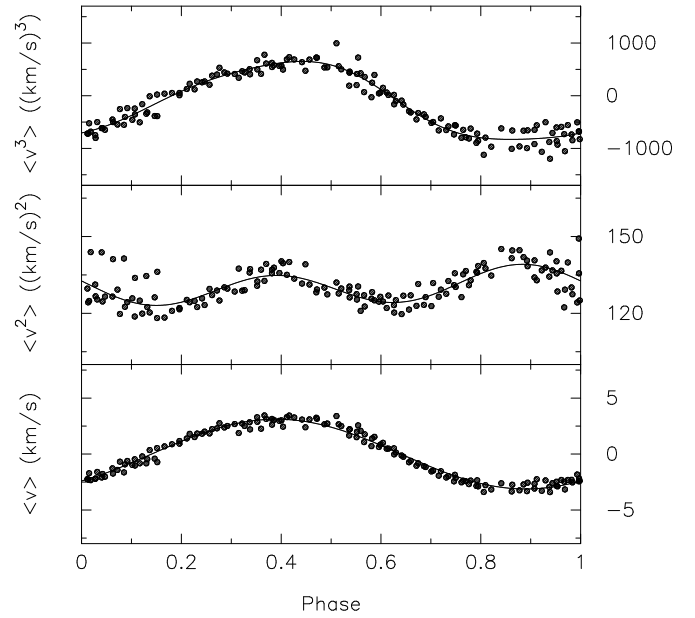


**Fig. 6.** The first three moments of the Fe I line at 6546.24 Å obtained on Feb. 21 and Feb. 24, 1995. Phases correspond to the frequency  $\nu_0$

**Table 2.** The different minima of the discriminant for  $\rho$  Pup corresponding to the frequency  $\nu_0$ .  $\gamma_\ell^m$ ,  $v_p$ ,  $v \sin i$ , and the width of the Gaussian intrinsic profile  $\sigma$  are given in  $\text{km.s}^{-1}$ .

$\ell$	$ m $	$\gamma_\ell^m$	$v_p$	$i$	$v \sin i$	$\sigma$
0	0	0.08	5.6	-	15.3	6.5
1	1	0.13	10.0	38°	14.8	5.9
2	1	0.17	12.1	64°	16.4	2.2
1	0	0.18	5.0	7°	19.6	1.7
2	2	0.23	15.0	53°	10.3	4.8
⋮	⋮	⋮	⋮	⋮	⋮	⋮

et al. 1977) and results in 0.039. The linear limb-darkening coefficient used is the one appropriate for the effective temperature and gravity of  $\rho$  Pup and amounts to 0.52 for the wavelength region that we are considering (Wade & Rucinski 1985). The results of the discriminant are presented in Table 1. We refer to Aerts (1996) for the interpretation of the parameters in Table 1. We clearly find a radial pulsation with an amplitude of  $5.6 \text{ km.s}^{-1}$ , well in agreement with previously known results. The  $v \sin i$  value is found to be  $15.3 \text{ km.s}^{-1}$  and the intrinsic broadening amounts to  $6.5 \text{ km.s}^{-1}$ . We find the same result for the main mode if we use the moments obtained with the blended 6546.24 Å line.

In order to investigate the nature of the modes with frequencies  $\nu_1$  and  $\nu_2$ , we have to consider the moments of the different nights. The first moment can easily be added for all the data shown in Figs. 5 and 6 since it is independent of the spectral line considered. The peak-to-peak amplitudes in the case of a triple periodic solution with  $\nu_0$ ,  $\nu_1$ , and  $\nu_2$  amount to respectively  $6.7 \pm 0.1$ ,  $0.9 \pm 0.1$ , and  $0.7 \pm 0.1 \text{ km.s}^{-1}$ . Comparing

these values with those given in Table 1 points out that the first moment leads to a larger amplitude for the two additional frequencies and a smaller one for the main frequency compared to the Gaussian fits to the profiles. This can be expected when the modes with frequencies  $\nu_1$  and  $\nu_2$  are non-radial, for which the variations in the wings are more important than for a radial mode. Therefore, the differences between these values and those of Table 1 reflect only the way the measurements of the velocity are derived from a given line.

Unlike the first moment, the higher order moments are dependent on the intrinsic broadening of the line. For the second moment, this dependence is limited to the constant term and therefore we can still easily add all  $\langle v^2 \rangle$ -data shown in Figs. 5 and 6 by shifting them such that their constant terms coincide. We then fitted the second moment by considering only the main frequencies  $\nu_i$  and  $2\nu_i$  ( $i = 0, 1, 2$ ). Such a fit explains 71% of the variance in the data. The reason for not taking into account all expected beat- and sum-frequencies (12 in total) is the too short time spread of our data, which then leads to inaccurately determined amplitudes. The dependence of the third moment on the spectral line is more complicated, but will not be considered here because we found that the complicated triple-periodic fit to the third moment is not sufficiently accurate to be of any value for the mode identification of the small-amplitude modes.

By using the information of the radial mode,  $v \sin i$  and  $\sigma$ , one may hope to determine the modes belonging to  $\nu_1$  and  $\nu_2$  by considering only the first two moments in the discriminant. The result is that the mode with frequency  $\nu_1$  is a low-degree axisymmetric mode ( $\ell \leq 3, m = 0$ ) and the one with frequency  $\nu_2$  is clearly non-axisymmetric ( $m \neq 0$ ). We are not able to definitely assign the wavenumbers to these modes, since several possibilities were found to be equivalent.

## 5. Search for a Van Hoof effect

One of the reasons why we applied for observing time for  $\rho$  Pup was to detect the wave propagation through the photospheric layers by looking at lines formed at different altitudes. Van Hoof & Struve (1953) noticed that for some  $\beta$  Cephei stars the velocity curves associated to each considered element could have different amplitudes and/or phases. This phenomenon has been called the Van Hoof effect and may have different interpretations. In particular, the Van Hoof effect can be the result of the running-wave character of the pulsation (Mathias & Gillet 1993). In a previous paper (Mathias & Aerts 1996) we tried to detect the Van Hoof effect in the  $\delta$  Scuti star 20 CVn. The result was not conclusive, mainly because of the very low 2K amplitude of this star ( $2K = 1.24 \pm 0.02 \text{ km.s}^{-1}$ ) associated with a non-radial primary pulsation mode. Since  $\rho$  Pup has one of the largest 2K amplitudes among the  $\delta$  Scuti stars and a main radial mode, the detection of the running wave effect should be easier in this star.

Following Mathias & Gillet (1993), we constructed several velocity-velocity diagrams. No “loop” structure appeared in the phase diagrams, the resulting curves having a width within the

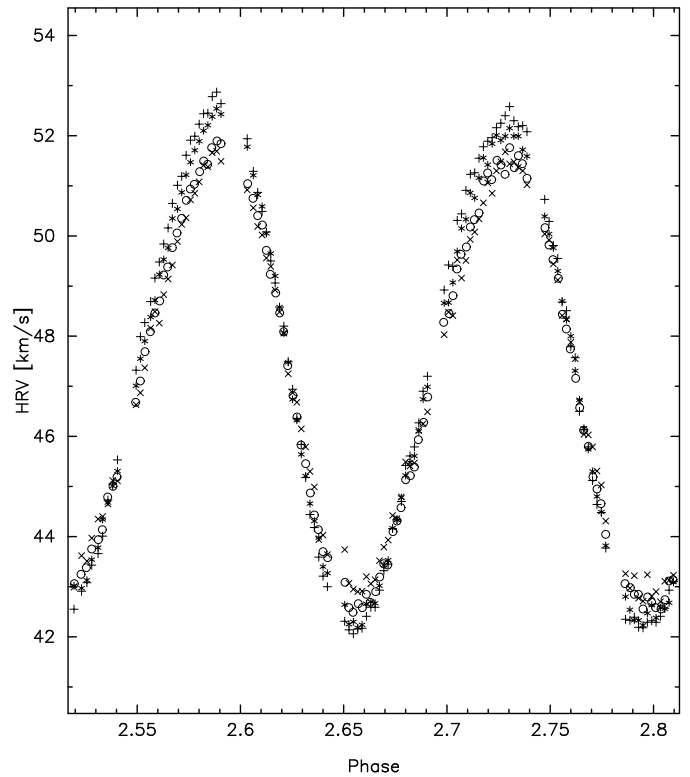


**Fig. 7.** Heliocentric velocity curves measured from the line bisector corresponding to the Ca I  $\lambda\lambda$  6122 line, obtained on February 23<sup>rd</sup>, 1995. The different symbols correspond to different line relative fluxes:  $\times$ : 20 %,  $\circ$ : 40 %,  $*$ : 70 % and  $+$ : 90 %. Note that a value of 100 % corresponds to the minimum of the line, and that 0 % corresponds to the continuum

error bars of the velocity. The radial-velocity curves used here were obtained through a gaussian fit on the whole profile. However, the line is formed along a certain optical depth, and the gaussian fit hence averages the velocity of the total line-forming region. If we suppose that a running wave effect is present, it might be non-detectable if the corresponding line-forming regions overlap. This might be the case for the  $\delta$  Scuti stars since their photosphere is not as extended as those of more evolved stars (e.g.  $\beta$  Cephei stars). Our results are the same if the center-of-mass (the first moment, see above) of the profile is used.

To avoid this problem, it is necessary to distinguish between the velocity associated with the deeper line-forming region (where the line wings are formed) and the one of the corresponding upper part (where the line core is formed). We therefore measured the velocity from the line bisector for different relative fluxes. We obtained radial-velocity curves as those represented on Fig. 7. The considered flux level influences the radial-velocity curve and the data are more dispersed just before the maximum than before the minimum i.e. just after the maximum radius. Such an asymmetry does not appear if the same study is performed on synthetic spectra, issued from computation of a radial mode with an infinitely thin line forming region. In this case, we find that, due to the projection effects, the larger

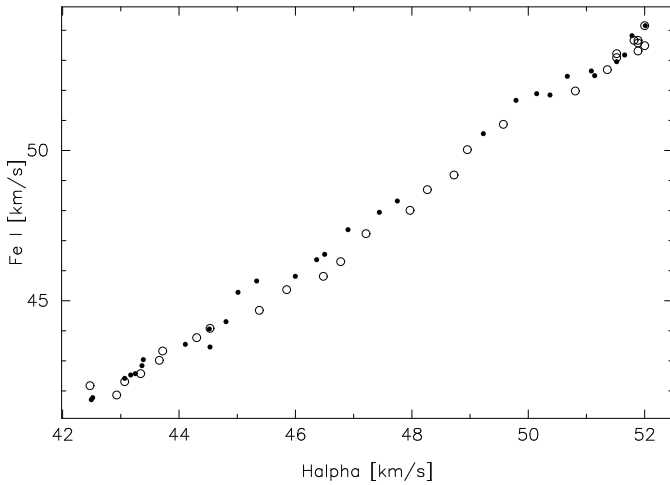


**Fig. 8.** The radial-velocity curve of Fe I  $\lambda\lambda$  6546 is represented versus that of H $\alpha$ . Both curves have been obtained through the line bisector method, measured at 90 % of the relative flux. Black dots represent the ascending branch of the heliocentric radial-velocity curve while the open circles stand for the descending branch. Hence, the diagram is drawn clockwise

the relative fluxes considered for the line bisector, the larger the corresponding velocity amplitude. The structure is the same around the minimum and the maximum of the radial-velocity curve. This asymmetry effect may be connected to the presence of non-radial oscillations (Aerts et al. 1994) or to the velocity gradient within the line forming region.

The velocity-velocity diagram was then drawn using the values at 90 % of the relative flux, considering the H $\alpha$  line on the one hand, and the two Fe I lines ( $\lambda\lambda$  6546 and 6569) on the other hand. In order to avoid problems due to the non-reproduction of the velocity curve from cycle to cycle, only data obtained between HJD 3.645654 and 3.774389 (from which 2 449 770 has been subtracted) were considered. The corresponding diagram is represented on Fig. 8. From this diagram, we can see that the black dots are slightly above the open circles. Because the diagram is drawn clockwise (see caption), the variation of the H $\alpha$  line is late compared to that of the Fe I  $\lambda\lambda$  6546 one. The width of the structure can then be calculated (Mathias & Gillet 1993) and the resulting time separation between the two variations is about  $58 \pm 19$  s. Hence, the running wave effect seems present in the pulsation of  $\rho$  Pup, inducing a propagation time of about 1 min to reach the core of the H $\alpha$  line from that of the Fe I  $\lambda\lambda$  6546 one. The above results are recovered if we consider the Fe I  $\lambda\lambda$  6569 line.

A larger propagation time should be found if we consider again the velocity curve of the H $\alpha$  line measured at 90 % and that of the Fe I  $\lambda\lambda$  6546 line, but measured this time at, for instance, 50 %. Indeed, in this case the wings of the Fe I line become more important in the determination of the velocity curve, and since they are formed deeper in the photosphere, the distance between the two measured variations is larger, and hence the propagation time as well. Surprisingly, the deduced propagation time is

found here to decrease with decreasing relative flux percentage. If the latter is below 70%, we find a negative propagation time, meaning that the deeper photosphere is late compared to the upper one. Such a result calls the following remarks:

- First, in our scenario, we postulate that the amplitude of the pulsation remains small enough to not produce a very extended and heterogeneous line-forming region. Indeed, using a theoretical approach, Albrow & Cottrell (1996) find out that the line function contributions based on static atmospheric models do not give a correct formation depth when the pulsation amplitude becomes too large, especially when shock waves develop within the atmosphere. Thus, we can expect that our results may be biased if large velocity gradients are present, since many absorption centers can alter the line profile.
- If a non-radial mode is present, we must expect that the line profile can be appreciably affected and causes an unreal running effect when we apply the line bisector method. Indeed using the parameters determined in Sect. 4, and assuming that only a radial mode exists, no “propagation time” should be measured if we consider the variations obtained from different percentages of the relative flux. Such an effect is, however, present if we consider a non-radial mode. In this case, the line bisector technique leads to a non-zero value of the time difference. Thus the latter is not a consequence of a running wave effect, but of the fact that considering a smaller relative flux value to derive the velocity curve is equivalent to limiting the integration area on the stellar disc in the line-of-sight for the computation of the lines.

We conclude that the line-bisector technique should be used with particular attention, in order to take into account all the phenomena which can affect the line profile. In our case, the most secure procedure is to compare the variations obtained for the same value of the line bisector (90 % here). Because a width of the velocity-velocity diagram is definitely present between the H $\alpha$  line and two Fe I lines, a running wave seems to be present in  $\rho$  Pup and shows the classical picture in which the hydrogen lines, formed in the upper atmosphere, are late compared to the metal lines if the wave is propagating outward.

## 6. The shock wave scenario

From medium-resolution spectra ( $\lambda/\Delta\lambda$  around 16 000, typical exposure time of 12 min), the authors in DLS infer that a shock wave mechanism is acting in  $\rho$  Pup. Their conclusion is based on the peculiar behaviour of the Ca II K line ( $\lambda\lambda$  3934), which shows a transient emission at the phase of maximum outward acceleration. The shock hypothesis has also been postulated for evolved  $\delta$  Scuti stars (e.g. Auvergne et al. 1979 and references therein) and is thought to be equivalent to the same mechanism at work in other variable classes such as W Virginis, RR Lyrae and classical Cepheid stars (e.g. Fokin, Gillet and Breittellner 1996). The shock causes emission which is observed for the hydrogen Balmer-lines in W Virginis and RR Lyrae stars, while it usually occurs in the Ca II H and K lines in classical Cepheids (although

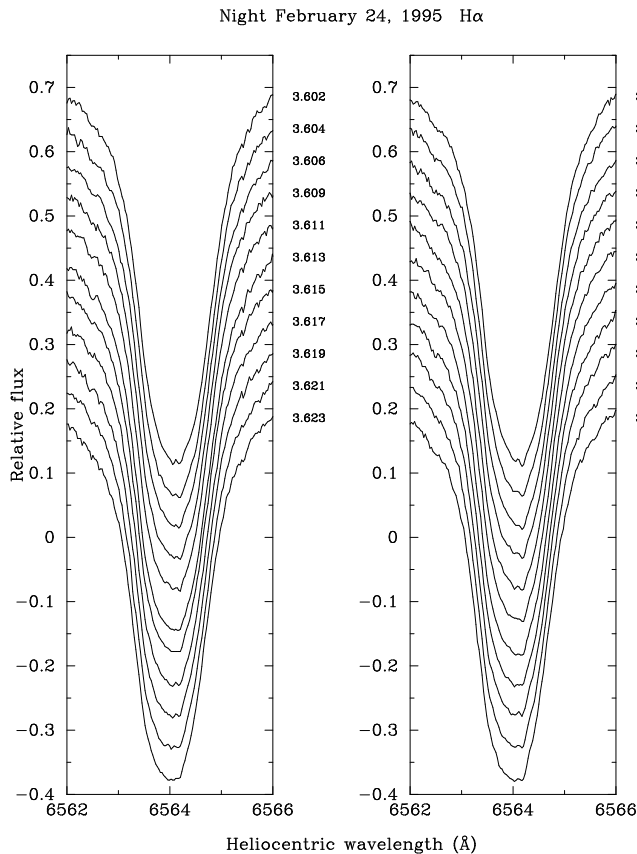


**Fig. 9.** The two sets of  $H\alpha$  profiles corresponding to our two consecutive cycles obtained on February 24<sup>th</sup>, 1995 (respectively left and right). The time, running downward, is indicated on the right hand side of each window and is expressed in heliocentric Julian days (from which 2 449 770 has been subtracted). Note that the spectra are not filtered

a weak blue emission component within the  $H\alpha$  absorption profile is observed in the longest periodic Cepheids).

In non-pulsating stars, the emission in the core of the Ca II K line is considered as a prominent indicator of the presence of stellar chromospheres. The detailed comparison of evolution of chromospheric emission profiles with non-LTE radiation hydrodynamic codes now provide very elaborate analysis for atmospheric dynamics (e.g. Carlsson and Stein, 1997). In their model of the structure of the solar chromosphere, Vernazza, Avrett and Loeser (1981) show that the core of the Ca II K and  $H\alpha$  lines are approximately formed in the same atmospheric region (see their Fig. 1). Thus we can expect that in pulsating stars, these two lines must be affected simultaneously by the pulsation.

In some pulsating stars such as the classical Cepheids, the presence of a chromospheric activity is well supported by permanent Ca II K and Mg II emission. Moreover Sasselov and Lester (1994a) report the first unambiguous detection throughout the whole pulsation cycle of the He I  $\lambda\lambda$  10830 absorption line in a few classical Cepheids. Today *self-consistent* non-linear non-adiabatic pulsating models exist with an extended atmosphere (e.g. Fokin, Gillet, Breittfeller 1996). Models of this

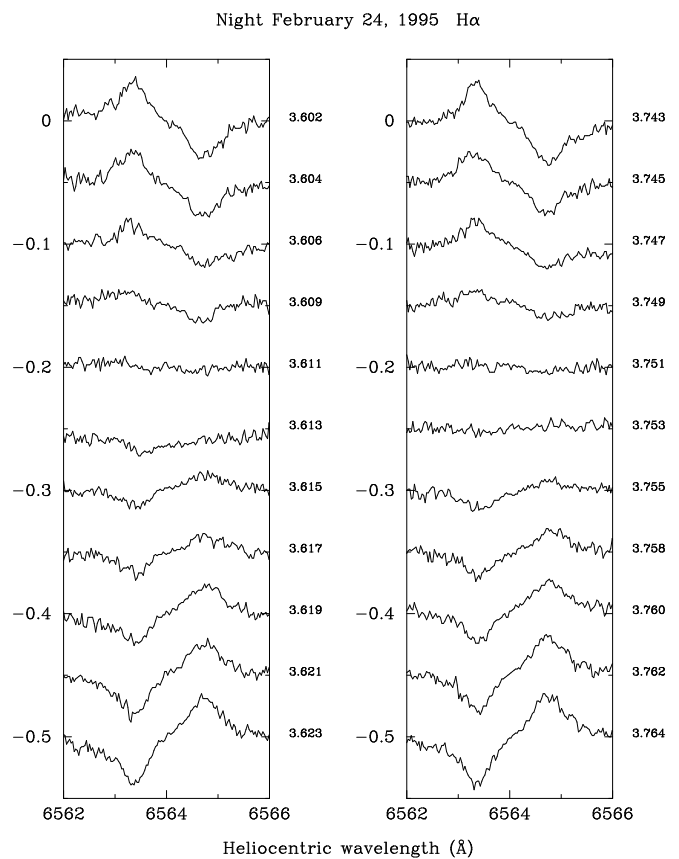


**Fig. 10.** Same as Fig. 9, but each spectrum has been subtracted from a mean spectrum, calculated using the spectra represented on each corresponding window represented on Fig. 9

type including a chromospheric structure are not yet available. Sasselov and Lester (1994b) have constructed an atmospheric pulsating model including a chromosphere. However, their pulsation mechanism is modeled by a driving piston instead of being induced by the  $\kappa$ - and  $\gamma$ -mechanisms, so the results of their model must be treated with caution. Nevertheless, they put into evidence the three main atmospheric shock waves obtained by Fokin, et al. (1996) during each pulsating cycle. Consequently, Sasselov and Lester's (1994b) work seems valid and it shows that pulsating stars can have chromospheres heated by acoustic (or magnetic) wave dissipation in addition to transient heating due to pulsational shocks depending on their intensity.

In  $\delta$  Scuti stars, and especially in  $\rho$  Pup, it is not obvious that the shock energy is large enough to induce a transient chromospheric heating because weak shocks are expected as shown by the very small radius amplitude  $\Delta R/R < 1\%$  (it is around 12–13% in classical Cepheids). Only the construction of a realistic pulsating chromospheric model of  $\rho$  Pup, which seems now possible to realize, would provide relevant information. However, such a model is beyond the scope of this paper.

In DLS a weak emission is present in the blue wing of the Ca II K line just before the maximum acceleration phase. Fig. 9 shows our  $H\alpha$  profiles around this phase. The time interval dis-

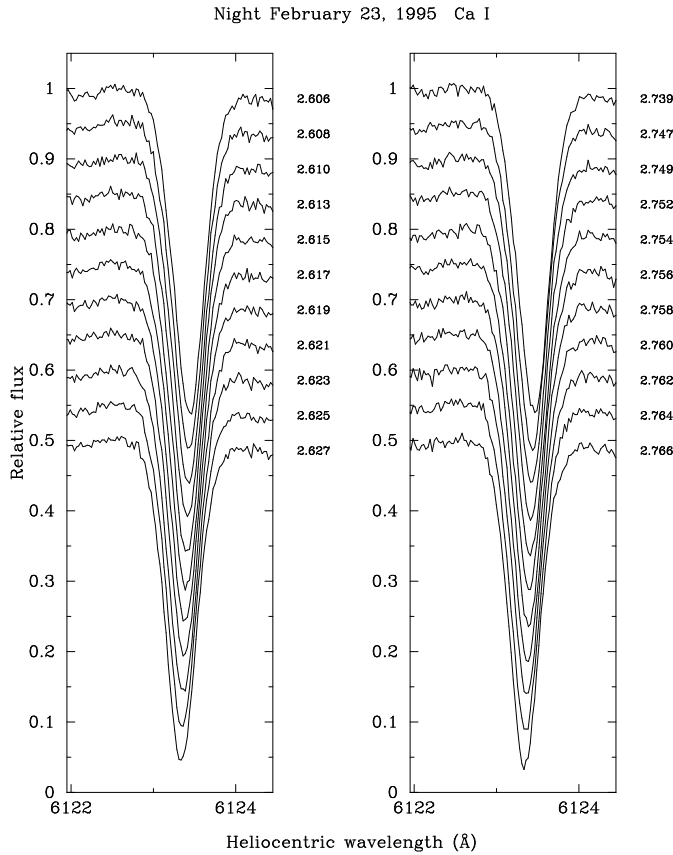


**Fig. 11.** Same as Fig. 9, but concerning the Ca I  $\lambda\lambda$  6122 line

played on this figure is about 1 h, well above the maximum estimated emission duration of less than 20 min given in DLS. It should be noted that this duration is relatively short compared to the one found in other classes of pulsating stars. In RR Lyr, the duration of the emission is about 40 minutes (Chadid, private communication). In the case of  $\rho$  Pup, the emission duration may be of the order of the time separating the middle of two consecutive observations, which is here about 3 min. Despite the high-quality of our data set, no structure can be seen on these profiles. The only one that shows a particular feature is that corresponding to HJD = 2 449 773.613 (Fig. 9). This spectrum appears deeper than the others, but it does not represent a small emission within the large absorption. The origin of this strange behaviour is not clear. The error of the normalisation of the continuum being less than 0.3 % in relative flux (while the measured difference, still in relative flux, between this spectrum and its neighbours is about 3 %), and the same mean flat-field having been used for all the displayed spectra, this phenomenon may be due to an instrumental effect. We also measured the widths related to the line bisector at different relative flux level. No sudden increase in the FWHM of the line is noted, as would be expected if a shock emission was present. Finally, we calculated the differential spectra (Fig. 10), but no sudden bump appears visible. Hence, no appreciable emission is detected at the  $H\alpha$  level. We performed a similar analysis on

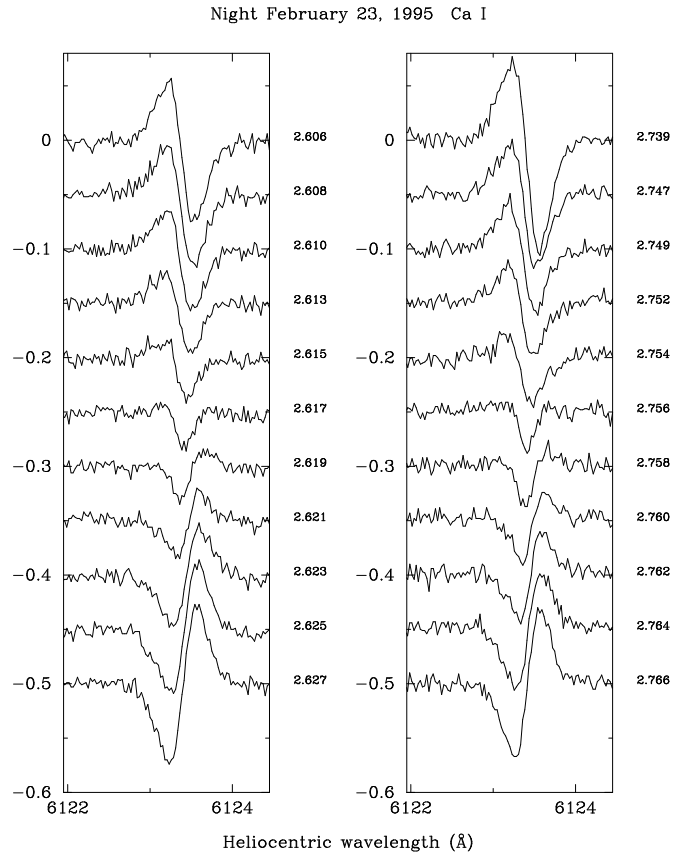


**Fig. 12.** Same as Fig. 10, but concerning the Ca I  $\lambda\lambda$  6122 line

the spectra corresponding to the Ca I profiles (Figs. 11 and 12) but here again, no structure connected to a possible filling-in emission has been detected.

Due to the non-reproducibility of the variations from cycle to cycle, we were perhaps unlucky to observe the star at the “wrong moment”. Indeed, it is noted in DLS that, during the cycle following the “emission” one, no similar phenomenon was seen. This observation cannot be attributed to the beat period since the secondary oscillation has a too weak velocity amplitude.

Finally, we conclude that we do not find any evidence to support a shock wave mechanism in  $\rho$  Pup from both hydrogen and metallic lines during our observed cycles. The lack of emission detection for  $H\alpha$  may be explained by the fact that the shock wave velocity remains too weak to provoke  $H\alpha$  emission. A *self-consistent* theoretical approach would be very helpful but, because the shock wave velocity is extremely sensitive to the dynamical state of the atmosphere and vice versa, a definitive answer seems difficult to obtain in this way. New simultaneous observations of Ca II K and  $H\alpha$  appear the best direction for further testing the shock wave scenario.

## 7. Conclusion

We used new high-quality spectroscopic data to study the pulsational behaviour of the  $\delta$  Scuti star  $\rho$  Pup. The radial-velocity curves deduced from different elements have a sinusoidal shape and are well reproduced with the frequency  $\nu_0$  derived by Ponsen (1963).

Small differences are observed between the velocity curves of different pulsation cycles. This is attributed to the presence of a secondary oscillation with a frequency around  $\nu_1 = 7.8 \text{ c.d}^{-1}$  having a small amplitude, and a possible third frequency around  $\nu_2 = 6.3 \text{ c.d}^{-1}$ .

The moment method was used to derive the pulsation parameters. As expected by the different studies available in the literature, the main mode is radial, with an intrinsic amplitude of  $5.6 \text{ km.s}^{-1}$ . The projected rotation velocity amounts to  $15.3 \text{ km.s}^{-1}$ . The secondary oscillation was found to be a small-amplitude low-degree axisymmetric mode, and, if real, the third oscillation is non-axisymmetric.

The study of the atmospheric dynamics shows that a running-wave effect may be present between the Fe I and  $\text{H}\alpha$  line, this latter being late by about 0.5 % of the pulsation period. The usual picture in which the  $\text{H}\alpha$  line-forming region is above that of the metal line, if we consider an outward running wave, is thus valid for this star.

Finally, from our observations of  $\text{H}\alpha$  and metallic line profiles, we have not found any clear evidence for the shock wave mechanism proposed in DLS. Two reasons, not exclusive, can account for that. First, the intensity of the expected shock wave is perhaps not strong enough to produce a  $\text{H}\alpha$  or metallic emission component while it can produce Ca II K emission. Because this latter does not occur during each pulsational cycle (DLS), the shock intensity must remain weak, at the limit of the excitation of the Ca II K line. Secondly, the presence of a transient emission can find its origin in a classical chromospheric activity which would not be directly connected to the pulsational motion and more particularly to the propagation of shock waves. Evidence of such a situation was given by Teays et al. (1989), who observed an increase in the Ca II K emission near minimum light of the  $\delta$  Scuti star  $\beta$  Cas.

It is important to note that the DLS scenario is mainly based on the presence of a single transient emission during the phase of maximum outward acceleration occurring at the maximum light. This is consistent with the observations of Fracassini et al. (1983) who detected a weak emission peak in the Mg II doublet near maximum light in  $\rho$  Pup. Such a coincidence is of course in favor of a shock wave propagation but it is clear that this well phased emission occurrence needs confirmation.

The observational status of  $\rho$  Pup remains not well-known (e.g. regarding the multiperiodicity), despite its large-amplitude variations. New data must be obtained for this object to refine the secondary period(s) and to point out the detailed pulsational behaviour. Especially, the Ca II K line should be accurately followed during several pulsation cycles in order to confirm the shock wave scenario of DLS. Because it is not easy to compute a *self-consistent* non-linear non-adiabatic pulsating model

including a chromospheric activity, an accurate observation of the Ca II K line actually seems the best way to verify the shock wave hypothesis.

*Acknowledgements.* The authors are indebted to Drs. D. Dravins and A.B. Fokin for fruitful discussions, and to the referee for constructive remarks.

## References

- Aerts, C. 1996, A&A 314, 115  
 Aerts, C., De Pauw, M., Waelkens, C. 1992, A&A 266, 294  
 Aerts, C., Mathias, P., Gillet, D., Waelkens, C. 1994, A&A 286, 109  
 Albrow, M.D., Cottrell, P.L. 1996, MNRAS 278, 344  
 Auvergne, M., Le Contel, J.-M., Baglin, A. 1979, A&A 76, 15  
 Balona, L.A. 1986, MNRAS 219, 111  
 Buscombe, W. 1957, Observatory 77, 144  
 Campos, A.J., Smith, M.A. 1980, ApJ 238, 667  
 Carlsson M., Stein R.F. 1997, ApJ 481, 500  
 Danziger, I.J., Kuhl, L.V. 1966, ApJ 146, 743  
 De Pauw, M., Aerts, C., Waelkens, C. 1993, A&A 280, 493  
 Dravins, D., Lind, J., Särg, K. 1977, A&A 54, 381 (DLS)  
 Eggen, O.J. 1956, PASP 68, 238  
 Fracassini, M., Pasinetti, L.E., Castelli, F., Antonello, E., Pastori, L. 1983, Ap&SS 97, 323  
 Fokin, A.B., Gillet, D., Breitfellner, M.G., 1996, A&A 307, 503  
 Kurtz, D.W., Garrison, R.F., Koen, C., Hofmann, G.F., Viranna, N.B. 1995, MNRAS 276, 199  
 Mathias, P., Gillet, D. 1993, A&A 278, 511  
 Mathias, P., Aerts, C. 1996, A&A 312, 905  
 Mathias, P., Aerts, C., De Pauw, M., Gillet, D., Waelkens, C. 1994, A&A 283, 813  
 Ponsen, J. 1963, BAN 17, 44  
 Roberts, D.H., Lehár, J., Dreher, J.W. 1987, ApJ 238, 946  
 Sasselov, D., Lester, J.B., 1994a, ApJ 423, 777  
 Sasselov, D., Lester, J.B., 1994b, ApJ 423, 795  
 Stumpff, P. 1980, A&AS 41, 1  
 Stellingwerf, R.F. 1978, ApJ 224, 953  
 Struve, O., Sahade, J., Zeberg, V. 1956, ApJ 124, 504  
 Teays, T.J., Schmidt, E.G., Fracassini, M., Pasinetti-Fracassini, L.E. 1989, ApJ 343, 916  
 Telting, J.H., Aerts, C., Mathias, P. 1997, A&A, in press  
 Trodahl, H.J., Sullivan, D.J. 1977, MNRAS 179, 209  
 Tsvetkov, Ts.G. 1984, IBVS 2523  
 Van Hoof, A., Struve, O. 1953, PASP 65, 158  
 Wade, R.A., Rucinski, S.M. 1985, A&AS 60, 471  
 Yang, S., Walker, G.A.H., Bennett, P. 1987, PASP 99, 425